

Backward single-pion production in the $pd \rightarrow {}^3\text{He} \pi^0$ reaction with WASA-at-COSY

The WASA-at-COSY Collaboration

P. Adlarson¹, W. Augustyniak², W. Bardan³, M. Bashkanov⁴, F.S. Bergmann⁵, M. Berłowski⁶, A. Bondar^{7,8}, M. Büscher^{9,10}, H. Calén¹, I. Ciepał¹¹, H. Clement^{12,13}, E. Czerwiński³, K. Demmich⁵, R. Engels¹⁴, A. Erven¹⁵, W. Erven¹⁵, W. Eyrich¹⁶, P. Fedorets^{14,17}, K. Föhl¹⁸, K. Fransson¹, F. Goldenbaum¹⁴, A. Goswami^{14,19}, K. Grigoryev^{14,20}, C.-O. Gullström¹, L. Heijkenkjöld^{1a}, V. Hejny¹⁴, N. Hüsken^{5b}, L. Jarczyk³, T. Johansson¹, B. Kamys³, G. Kemmerling^{15c}, G. Khatri^{3d}, A. Khoukaz⁵, A. Khreptak³, D.A. Kirillov²¹, S. Kistryn³, H. Kleines^{15e}, B. Klos²², W. Krzemień⁶, P. Kulesa¹¹, A. Kupść^{1,6}, A. Kuzmin^{7,8}, K. Lalwani²³, D. Lersch¹⁴, B. Lorentz¹⁴, A. Magiera³, R. Maier^{14,24}, P. Marciniowski¹, B. Mariański², H.-P. Morsch², P. Moskal³, H. Ohm¹⁴, W. Parol¹¹, E. Perez del Rio^{12,13f}, N.M. Piskunov²¹, D. Prasuhn¹⁴, D. Pszczel^{1,6}, K. Pysz¹¹, A. Pyszniak^{1,3}, J. Ritman^{14,24,25}, A. Roy¹⁹, Z. Rudy³, O. Rundel³, S. Sawant²⁵, S. Schadmand¹⁴, I. Schätti-Ozerianska³, T. Sefzick¹⁴, V. Serdyuk¹⁴, B. Shwartz^{7,8}, K. Sitterberg⁵, T. Skorodko^{12,13,27}, M. Skurzok³, J. Smyrski³, V. Sopov¹⁷, R. Stassen¹⁴, J. Stepaniak⁶, E. Stephan²², G. Sterzenbach¹⁴, H. Stockhorst¹⁴, H. Ströher^{14,24}, A. Szczurek¹¹, A. Trzciński², M. Wolke¹, A. Wrońska³, P. Wüstner¹⁵, A. Yamamoto²⁸, J. Zabierowski³⁹, M.J. Zieliński³, J. Złomańczuk¹, P. Żuprański², M. Żurek¹⁴, and C. Wilkin³⁰

- ¹ Division of Nuclear Physics, Department of Physics and Astronomy, Uppsala University, Box 516, 75120 Uppsala, Sweden
- ² Department of Nuclear Physics, National Centre for Nuclear Research, ul. Hoza 69, 00-681, Warsaw, Poland
- ³ Institute of Physics, Jagiellonian University, prof. Stanisława Łojasiewicza 11, 30-348 Kraków, Poland
- ⁴ School of Physics and Astronomy, University of Edinburgh, James Clerk Maxwell Building, Peter Guthrie Tait Road, Edinburgh EH9 3FD, United Kingdom
- ⁵ Institut für Kernphysik, Westfälische Wilhelms-Universität Münster, Wilhelm-Klemm-Str. 9, 48149 Münster, Germany
- ⁶ High Energy Physics Department, National Centre for Nuclear Research, ul. Hoza 69, 00-681, Warsaw, Poland
- ⁷ Budker Institute of Nuclear Physics of SB RAS, 11 akademika Lavrentieva prospect, Novosibirsk, 630090, Russia
- ⁸ Novosibirsk State University, 2 Pirogova Str., Novosibirsk, 630090, Russia
- ⁹ Peter Grünberg Institut, PGI-6 Elektronische Eigenschaften, Forschungszentrum Jülich, 52425 Jülich, Germany
- ¹⁰ Institut für Laser- und Plasmaphysik, Heinrich-Heine Universität Düsseldorf, Universitätsstr. 1, 40225 Düsseldorf, Germany
- ¹¹ The Henryk Niewodniczański Institute of Nuclear Physics, Polish Academy of Sciences, Radzikowskiego 152, 31-342 Kraków, Poland
- ¹² Physikalisches Institut, Eberhard-Karls-Universität Tübingen, Auf der Morgenstelle 14, 72076 Tübingen, Germany
- ¹³ Kepler Center für Astro- und Teilchenphysik, Physikalisches Institut der Universität Tübingen, Auf der Morgenstelle 14, 72076 Tübingen, Germany
- ¹⁴ Institut für Kernphysik, Forschungszentrum Jülich, 52425 Jülich, Germany
- ¹⁵ Zentralinstitut für Engineering, Elektronik und Analytik, Forschungszentrum Jülich, 52425 Jülich, Germany
- ¹⁶ Physikalisches Institut, Friedrich-Alexander-Universität Erlangen-Nürnberg, Erwin-Rommel-Str. 1, 91058 Erlangen, Germany
- ¹⁷ Institute for Theoretical and Experimental Physics named after A.I. Alikhanov of National Research Centre “Kurchatov Institute”, 25 Bolshaya Chermushkinskaya, Moscow, 117218, Russia

^a present address: Institut für Kernphysik, Johannes Gutenberg-Universität Mainz, Johann-Joachim-Becher Weg 45, 55128 Mainz, Germany

^b Email: n.hues02@uni-muenster.de

^c present address: Jülich Centre for Neutron Science JCNS, Forschungszentrum Jülich, 52425 Jülich, Germany

^d present address: Department of Physics, Harvard University, 17 Oxford St., Cambridge, MA 02138, USA

^e present address: Jülich Centre for Neutron Science JCNS, Forschungszentrum Jülich, 52425 Jülich, Germany

^f present address: INFN, Laboratori Nazionali di Frascati, Via E. Fermi, 40, 00044 Frascati (Roma), Italy

- ¹⁸ II. Physikalisches Institut, Justus-Liebig-Universität Gießen, Heinrich-Buff-Ring 16, 35392 Giessen, Germany
¹⁹ Department of Physics, Indian Institute of Technology Indore, Khandwa Road, Simrol, Indore - 453552, Madhya Pradesh, India
²⁰ High Energy Physics Division, Petersburg Nuclear Physics Institute named after B.P. Konstantinov of National Research Centre “Kurchatov Institute”, 1 mkr. Orlova roshcha, Leningradskaya Oblast, Gatchina, 188300, Russia
²¹ Veksler and Baldin Laboratory of High Energy Physics, Joint Institute for Nuclear Physics, 6 Joliot-Curie, Dubna, 141980, Russia
²² August Chelkowski Institute of Physics, University of Silesia, Uniwersytecka 4, 40-007, Katowice, Poland
²³ Department of Physics, Malaviya National Institute of Technology Jaipur, JLN Marg Jaipur - 302017, Rajasthan, India
²⁴ JARA-FAME, Jülich Aachen Research Alliance, Forschungszentrum Jülich, 52425 Jülich, and RWTH Aachen, 52056 Aachen, Germany
²⁵ Institut für Experimentalphysik I, Ruhr-Universität Bochum, Universitätsstr. 150, 44780 Bochum, Germany
²⁶ Department of Physics, Indian Institute of Technology Bombay, Powai, Mumbai - 400076, Maharashtra, India
²⁷ Department of Physics, Tomsk State University, 36 Lenina Avenue, Tomsk, 634050, Russia
²⁸ High Energy Accelerator Research Organisation KEK, Tsukuba, Ibaraki 305-0801, Japan
²⁹ Astrophysics Division, National Centre for Nuclear Research, Box 447, 90-950 Łódź, Poland
³⁰ Physics and Astronomy Department, UCL, Gower Street, London WC1E 6BT, United Kingdom

Received: date / Revised version: date

Abstract. New data on the production of single neutral pions in the $pd \rightarrow {}^3\text{He}\pi^0$ reaction are presented. For fifteen proton beam momenta between $p_p = 1.60$ GeV/ c and $p_p = 1.74$ GeV/ c , differential cross sections are determined over a large fraction of the backward hemisphere. Since the only previous systematic measurements of single-pion production at these energies were made in collinear kinematics, the present work constitutes a significant extension of the current knowledge on this reaction. Even this far above the production threshold, significant changes are found in the behaviour of the angular distributions over small intervals in beam momentum.

1 Introduction

In contrast to other meson production reactions in proton-deuteron fusion, most notably the η - and $(\pi\pi)^0$ -channels, the production of single, neutral pions in the reaction $pd \rightarrow {}^3\text{He}\pi^0$ is considerably less well-studied in the energy region around the η -production threshold. Early measurements of the cross section (see Fig. 1) and tensor analysing power of the pd (dp) $\rightarrow {}^3\text{He}\pi^0$ and $pd \rightarrow {}^3\text{H}\pi^+$ reactions in collinear kinematics with the SPES4 spectrometer at SATURNE [3, 4] revealed strong structures in both observables for backward pion production (with respect to the direction of the incident proton in the c.m. frame) around $p_p = 1.70$ GeV/c. It is important to note here that, since there is only one isospin amplitude, the cross section for $pd \rightarrow {}^3\text{H}\pi^+$ should be twice that for $pd \rightarrow {}^3\text{He}\pi^0$, though deviations of the order of 10% have been reported in the literature [1, 2].

Apart from a single measurement of $dp \rightarrow {}^3\text{He}\pi^0$ at $p_d = 3.5$ GeV/c [5], angular distributions in the η -threshold region have so far remained largely unexplored. Nevertheless, the extensive database of cross sections for collinear production, combined with the similarities of the ${}^3\text{He}$ detection in the reactions $pd \rightarrow {}^3\text{He}\eta$ and $pd \rightarrow {}^3\text{He}\pi^0\pi^0$, have made $pd \rightarrow {}^3\text{He}\pi^0$ a prime candidate for luminosity determinations in fusion reactions [6, 7]. There is, thus, a twofold motivation for extended studies of differential cross sections of the $pd \rightarrow {}^3\text{He}\pi^0$ reaction. These will permit an exploration of the variations close to $\cos\vartheta_{\pi^0}^* = -1$ in the vicinity of the η -production threshold as well as the establishment of a new database for future experiments, that does not rely on an extrapolation to collinear kinematics. Data obtained in parallel

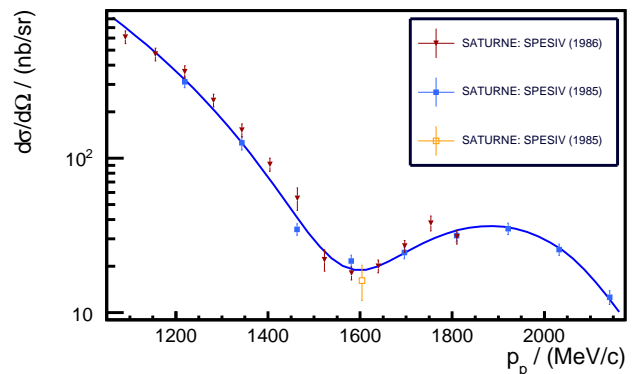


Fig. 1. Differential cross sections of the reactions $pd \rightarrow {}^3\text{He}\pi^0$ and $pd \rightarrow {}^3\text{H}\pi^+$ (scaled by an isospin factor of 0.5) at $\cos\vartheta_{\pi^0}^* = -1$ [3, 4]. The curve represents a fourth order polynomial fit to the combined database.

to the WASA-at-COSY experiment on η -production away from threshold [8] allow a detailed study of the cross sections for single-pion production over a large part of the backward hemisphere.

2 Experiment

The π^0 data were obtained at the WASA facility located within the Cooler Synchrotron (COSY) of the Forschungszentrum Jülich in the same experiment as that designed to study η production [8]. Beam protons were steered to collide with pellets of frozen deuterium so that the heavy

${}^3\text{He}$ ejectiles were emitted near the forward direction in the laboratory frame. The WASA Forward Detector allows the energy and the polar and azimuthal angles of the ${}^3\text{He}$ nuclei to be reconstructed in multiple layers of plastic scintillators and a proportional chamber, respectively. Detailed information on the experimental setup can be found in Ref. [9]. Fifteen evenly spaced proton beam momenta were used between $p_p = 1.60$ GeV/ c and $p_p = 1.74$ GeV/ c , with a resolution of $\Delta p/p \approx 10^{-3}$ [10]. Utilising the so-called supercycle mode of the accelerator, data can be taken at eight different beam momentum settings, with multiple repeats one after another, thus minimising systematic differences between the individual measurements. In practice, two such supercycles were employed in this experiment. The measurement at $p_p = 1.70$ GeV/ c was repeated in both supercycles and an additional single-momentum measurement was made at 1.70 GeV/ c to allow systematic effects between the two supercycles to be investigated.

3 Analysis

The ${}^3\text{He}$ nuclei produced near the forward direction are identified in the WASA Forward Detector by means of their energy loss. From this energy loss, a first value of the kinetic energy $T_{3\text{He}}$ can be estimated by comparison with a Monte Carlo simulation of the π^0 production reaction. By measuring also the polar and azimuthal scattering angles ϑ and φ in the Forward Proportional Chamber, the four-momenta of the ${}^3\text{He}$ nuclei are fully determined so that a missing-mass analysis can be performed. The analytic relation between the precisely measured polar scattering angle ($\Delta\vartheta \approx 0.2^\circ$) and the kinetic energy of ${}^3\text{He}$ nuclei was exploited in order to carefully monitor the energy calibration (see Fig. 2).

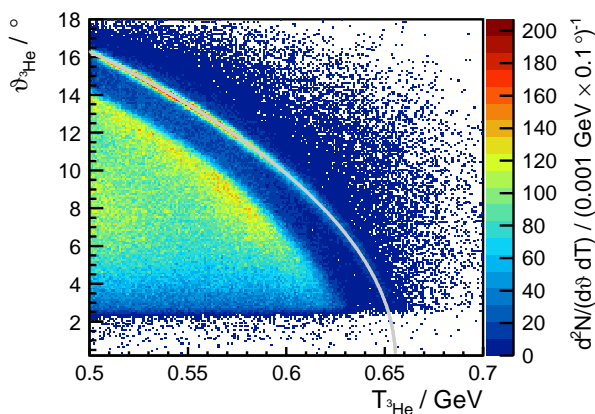


Fig. 2. Production angle of ${}^3\text{He}$ nuclei in the laboratory frame displayed as a function of its kinetic energy. The two-dimensional plot represents data (with color indicating the event yield) whereas the grey line follows from applying four-momentum conservation to the $pd \rightarrow {}^3\text{He}\pi^0$ reaction.

For the study reported here, only the ${}^3\text{He}$ in the final state was used, even though the detector system was also capable of measuring photons from the decay of the π^0 . A missing-mass analysis allowed the angular distribution of single-pion production to be derived from the final state momentum spectra binned in $\cos\vartheta_{\pi^0}^*$. An example of such a final state momentum spectrum, with a bin-width of $\Delta\cos\vartheta_{\pi^0}^* = 0.016$, can be found in Fig. 3. The background, largely associated with two-pion production and single-pion production with a poorly reconstructed energy due to the breakup of ${}^3\text{He}$ nuclei in the scintillator material, is subtracted using a fit of the type

$$f(x) = e^{a(x-0.5)}(b + cx + dx^2), \quad (1)$$

where x is the ${}^3\text{He}$ c.m. momentum. The fit is made outside the peak region. The effect of nuclear breakup of the ${}^3\text{He}$ within the detector is accounted for in a Monte Carlo simulation using an extension to GEANT3 [11], originally developed for the work in Ref. [12]. A fit of a Gaussian to the background-subtracted data is used to define a $\pm 3\sigma$ environment around the peak position. The event yield within a certain bin in $\cos\vartheta_{\pi^0}^*$ is then defined as the integral of the background-subtracted data in the $\pm 3\sigma$ interval.

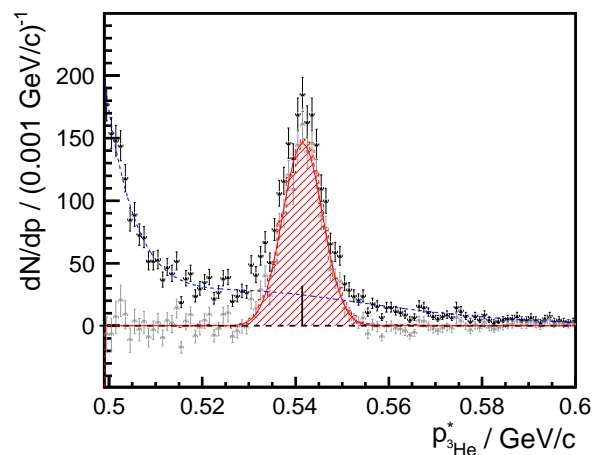


Fig. 3. Spectrum of the final state momentum $p_{3\text{He}}^*$ of ${}^3\text{He}$ nuclei in the centre-of-mass system for $-0.856 \leq \cos\vartheta_{\pi^0}^* < -0.840$ at a laboratory beam momentum of $p_p = 1.70$ GeV/ c . Black upward triangles represent data. The blue dashed line is a fit of the type given in Eq. (1) to the spectrum, excluding the peak region. Grey downward triangles show the data after subtraction of the background fit. The π^0 peak is fitted by a Gaussian distribution (continuous red line) and compared to a Monte Carlo simulation of the $pd \rightarrow {}^3\text{He}\pi^0$ reaction (red shaded histogram). The nominal peak position for a beam momentum of $p_p = 1.70$ GeV/ c is indicated by the upright, solid black line.

As no information is available on the angular distribution of single-pion production, the product of acceptance and reconstruction efficiency (for simplicity called

below the acceptance $A(\cos\vartheta_{\pi^0}^*)$ is first derived from a Monte Carlo simulation of π^0 production, assuming that the events are uniformly distributed over phase-space. The angular distributions found in the experiment are corrected for the acceptance by bin-wise multiplication with $A^{-1}(\cos\vartheta_{\pi^0}^*)$. A polynomial fit of fourth order to these distributions is subsequently used to weight the Monte Carlo simulations. This procedure is repeated until there is convergence of $A(\cos\vartheta_{\pi^0}^*)$, when the angular distributions are determined. This method was applied separately for the measurements at all 15 beam momenta.

Examples of the resulting acceptance as function of $\cos\vartheta_{\pi^0}^*$ are displayed in Fig. 4 for the measurements at 1.60 GeV/c, 1.70 GeV/c and 1.74 GeV/c. At very large negative values of $\cos\vartheta_{\pi^0}^*$, the beam pipe in the detector limits the acceptance, whereas for the smallest value of $\vartheta_{\pi^0}^*$ the polar production angle $\vartheta_{3\text{He}}$ exceeds the geometrical coverage of the Forward Detector. On average, the angle-dependent acceptance $A(\cos\vartheta_{\pi^0}^*)$ is of the order of 40%. This relatively small value is due mainly to the nuclear breakup of the ${}^3\text{He}$ ions in the scintillator, leading to either a misidentification or a poorly reconstructed kinetic energy.

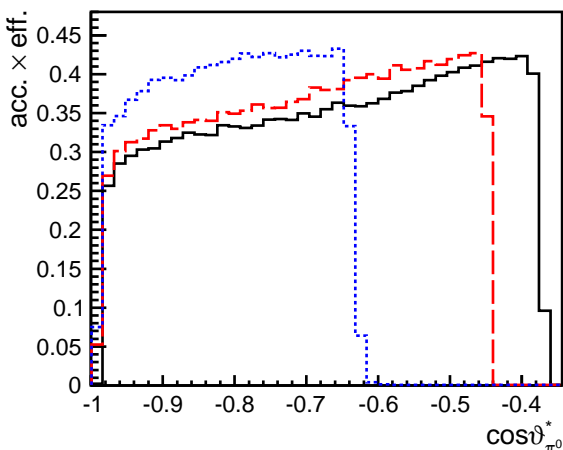


Fig. 4. Product of acceptance and reconstruction efficiency $A(\cos\vartheta_{\pi^0}^*)$ for the $pd \rightarrow {}^3\text{He}\pi^0$ reaction as function of the c.m. production angle for beam momenta of $p_p = 1.60$ GeV/c (blue, short-dashed line), $p_p = 1.70$ GeV/c (red long-dashed line) and $p_p = 1.74$ GeV/c (black, solid line).

4 Normalisation

Since the data reported here were taken in parallel to those used to investigate η production in pd -fusion, the same normalisation methodology can be applied [8], and this is briefly summarised. A first relative normalisation is derived from the ratio of protons elastically scattered off the target deuteron at a certain beam momentum and the reference momentum $p_p = 1.70$ GeV/c. The luminosity for the measurement at $p_p = 1.70$ GeV/c is obtained

by normalisation to the measured $pd \rightarrow {}^3\text{He}\eta$ total cross section [13]. The statistical uncertainty of the luminosity determination is of the order of 2% but an additional systematic normalisation uncertainty of $\approx 16\%$ needs to be considered. For more information on the normalisation procedure, the reader is referred to Refs. [8,14].

5 Results

The angular distributions of single-pion production in proton-deuteron fusion are converted into the differential cross sections shown in Fig. 5 using the luminosities previously derived [8,14]. Apart from the normalisation, the two main sources of the remaining systematic uncertainty, shown by the grey histogram in Fig. 5, are minor imprecisions in the determination of the polar production angle (with a possible offset of $\pm 0.04^\circ$) and the distribution of residual gas within the WASA scattering chamber. However, a comparison with the available data for collinear production reveals a good agreement, especially if the normalisation uncertainties of both the present data and those from the Saclay experiments [3,4] are taken into account. To show this more clearly, the combined normalisation uncertainty is incorporated into the error bars of the grey circles in Fig. 5.

The data shown in Fig. 5 can be well fit with the fourth order polynomial

$$\frac{d\sigma}{d\Omega} = \sum_{n=0}^{n=4} a_n (\cos\vartheta_{\pi^0}^* + 1)^n \quad (2)$$

and the values of the parameters a_n are to be found in Table 1 for the fifteen different beam momenta. Error bars are not shown because they are very misleading in view of the very strong correlations between the parameters. Nevertheless, the parametrisation of the data with Eq. (2) gives a good description of our results that can be used in the normalisation of other experiments.

For all the data above about 1.66 GeV/c there is clear evidence for a minimum in the differential cross section close to $\cos\vartheta_{\pi^0}^* = -1$. However, the fit parameters of Table 1 show that at lower momenta there may also be a minimum but that it is in the unphysical region of $\cos\vartheta_{\pi^0}^* < -1$. The minimum therefore moves somewhat with beam momentum from $\cos\vartheta_{\pi^0}^* \approx -1.1$ at $p_p = 1.62$ GeV/c to -0.93 at 1.74 GeV/c. In contrast, the maximum seen in Fig. 5 hardly moves from its position at $\cos\vartheta_{\pi^0}^* \approx -0.61$.

In general, six independent helicity amplitudes are required to describe completely the $pd \rightarrow {}^3\text{He}\pi^0$ reaction. These reduce to two, A and B , in the forward and backward directions and the magnitudes of these, $|A|^2$ and $|B|^2$, can be deduced from the Saclay measurements of the differential cross section and deuteron tensor analysing power T_{20} [4]. At $\vartheta_{\pi^0}^* = 180^\circ$ both $|A|^2$ and $|B|^2$ show minima for proton beam momenta around 1600 to 1650 MeV/c. This behaviour, which causes rapid variations in T_{20} , must clearly be linked to the moving minima seen in our data shown in Fig. 5.

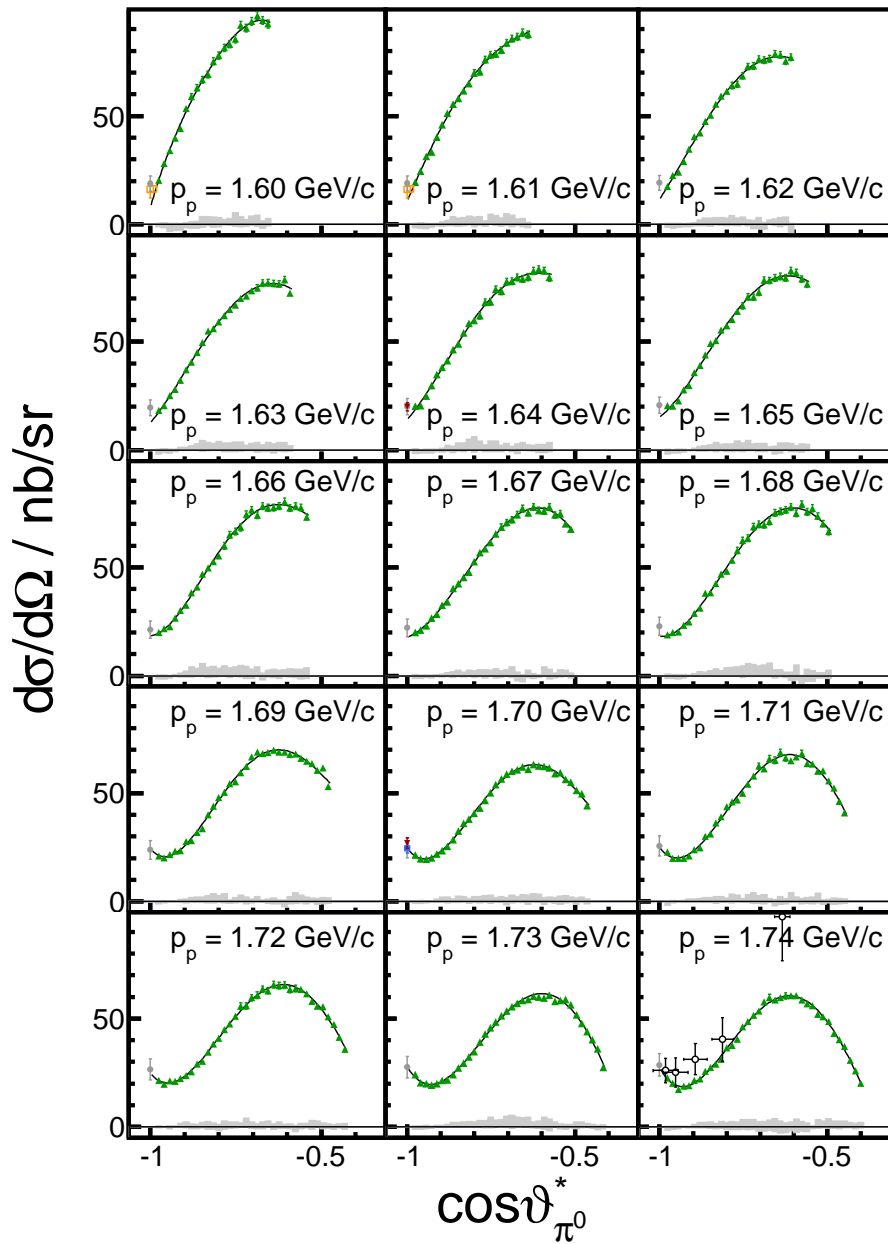


Fig. 5. Differential cross sections of the $pd \rightarrow {}^3\text{He}\pi^0$ reaction in the backward hemisphere for the different values of the beam momentum p_p noted in each panel. Green upward triangles represent the present data, yellow empty boxes a measurement at $p_p = 1.604$ GeV/c [3], the blue filled box a measurement of $pd \rightarrow {}^3\text{H}\pi^+$ at $p_p = 1.697$ GeV/c (scaled by an isospin factor of 0.5) [3], red downward triangles the measurements of $dp \rightarrow {}^3\text{He}\pi^0$ at $p_d = 3.276$ GeV/c and $p_d = 3.392$ GeV/c [4], and the black empty circles the measurement of $dp \rightarrow {}^3\text{He}\pi^0$ at $p_d = 3.50$ GeV/c [5]. In addition, the grey filled circles represent the values of a fit to the combined database shown in Fig. 1 at the appropriate beam momentum. In the last case the error bars are composed of the statistical uncertainty of the fit as well as of the normalisation uncertainty of both the present experiment and the literature data. Black solid lines represent fits of the type given in Eq. (2). Normalisation uncertainties of the individual datasets are not displayed. The grey histograms represent the systematic uncertainties, other than normalisation, of the present measurements.

Table 1. Values of the parameters a_n obtained from fits to our data using Eq. (2) for the different beam momenta.

p_p GeV/c	a_0 nb/sr	a_1	a_2	a_3	a_4	χ^2/ndf
1.60	7.99	548	-1566	4124	-6096	14.0/16
1.61	10.83	358	-122	-1447	1910	12.2/17
1.62	11.63	231	523	-2585	2117	16.4/19
1.63	12.65	190	645	-2464	1608	16.0/20
1.64	14.25	171	793	-2918	2294	19.9/21
1.65	15.25	114	1024	-3053	1968	28.0/22
1.66	18.47	10	1787	-5147	3886	17.3/23
1.67	17.92	49	1067	-2433	960	12.5/25
1.68	18.38	-30	1610	-3776	2155	27.4/26
1.69	24.43	-188	2612	-6461	4528	32.7/27
1.70	24.43	-200	2392	-5601	3680	35.8/28
1.71	25.04	-203	2316	-4978	2807	36.1/29
1.72	24.67	-188	2199	-4779	2743	16.2/30
1.73	27.70	-254	2259	-4434	2255	27.5/31
1.74	27.47	-285	2621	-5545	3230	25.8/32

It may also be relevant that the proton analysing power in the $\bar{p}d \rightarrow {}^3\text{He}\pi^0$ reaction at fixed pion angle of $\vartheta_{\pi^0}^* = 170^\circ$ shows an extremely rapid variation with the proton beam momentum in the 1600 MeV/c region [15]. There is therefore much structure in large angle $pd \rightarrow {}^3\text{He}\pi^0$ data near the η threshold and it is tempting to wonder whether this is more than an accident.

The amplitude for the $pd \rightarrow {}^3\text{He}\eta$ reaction near threshold is anomalously strong [16,17] and might be an indication of the formation of a quasibound ${}^3_\eta\text{He}$ state [18]. There might therefore be an extra S -wave contribution caused by η production followed by the transmutation $\eta{}^3\text{He} \rightarrow {}^3\text{He}\pi^0$ that will interfere with a direct mechanism. However, using data on $\pi^-{}^3\text{He} \rightarrow {}^3\text{H}\eta$ [19], it seems that this two-step approach may be too small to explain the backward minima. However, there is no valid reason to retain only the ${}^3\text{He}$ ground state in the intermediate state. Further theoretical work will be needed to explore this interesting region.

6 Summary

Measurements of the differential cross sections of single-pion production in proton-deuteron fusion have been here reported for fifteen different proton beam momenta between 1.60 GeV/c and 1.74 GeV/c. These data, which cover a large part of the backward hemisphere, are a significant extension of the current database that contained only detailed information for collinear production. Despite the data being taken far above the π^0 production threshold, where the excess energy is limited by $426 \text{ MeV} < Q_{\pi^0} < 494 \text{ MeV}$, there are important changes in the angular distributions with increasing Q_{π^0} . In particular at the lowest energy the large angle minimum is at an unphysical point but it becomes observable with rising Q_{π^0} . This and other phenomena [4,15] seem to occur close to the threshold for η production. It will require much more theoretical work to see if this is more than a coincidence.

Irrespective of the interpretation of the observed angular distributions, the new data will be a valuable tool for normalising the cross sections for other meson production reactions in proton-deuteron fusion. These data, which are parametrised in Eq. (2) and Table 1, will avoid having to rely on any extrapolation to collinear kinematics.

Acknowledgements

The work presented here received funding from the European Union Seventh Framework Programme (FP7/2007-2013) under grant agreement number 283286. The support given by the Forschungszentrum Jülich FFE Funding Programme of the Jülich Centre for Hadron Physics, by the Polish National Science Centre through grant No. 2016/23/B/ST2/00784, and by the DFG through the Research Training Group GRK2149 is gratefully acknowledged. We thank the COSY crew for their work and the excellent conditions made available during the beam time.

References

1. J.W. Low et al., Phys. Rev. C **23**, 1656 (1981).
2. E. Aslanides et al., Phys. Rev. Lett. **39**, 1654 (1977).
3. P. Berthet et al., Nucl. Phys. A **443**, 589 (1985). doi: 10.1016/0375-9474(85)90215-5
4. C. Kerboul et al., Phys. Lett. B **181**, 28 (1986). doi: 10.1016/0370-2693(86)91248-7
5. J. Banaigs et al., Phys. Lett. B **45**, 394 (1973). doi: 10.1016/0370-2693(73)90063-4
6. P. Adlarson et al., Eur. Phys. J. A **50**, 100 (2014). doi: 10.1140/epja/i2014-14100-4, arXiv:1402.3469 [nucl-ex]
7. P. Adlarson et al., Phys. Rev. C **91**, 015201 (2015). doi: 10.1103/PhysRevC.91.015201, arXiv:1408.5744 [nucl-ex]
8. P. Adlarson et al., arXiv:1801.06671 [nucl-ex].
9. H.-H. Adam et al., *Proposal for the wide angle shower apparatus (WASA) at COSY-Jülich: WASA at COSY*, (2004), arXiv: nucl-ex/0411038
10. R. Maier, Nucl. Instrum. Meth. A **390**, 18 (1997). doi:10.1016/S0168-9002(97)00324-0
11. R. Brun et al., *GEANT Detector Description and Simulation Tool*, (1994), https://cds.cern.ch/record/1082634/files/geantall_CERN-W5013.pdf
12. R. Bilger et al., Phys. Rev. C **65**, 044608 (2002). doi: 10.1103/PhysRevC.65.044608
13. T. Rausmann et al., Phys. Rev. C **80**, 017001 (2009). doi: 10.1103/PhysRevC.80.017001, arXiv:0905.4595 [nucl-ex]
14. N. Hüskens, *η and π^0 production in proton-deuteron fusion to ${}^3\text{He}X$ with WASA-at-COSY*, PhD thesis (2017), Westfälische Wilhelms-Universität Münster, Germany
15. B. Mayer et al., Phys. Lett. B **181**, 25 (1986).
16. J. Smyrski et al., Phys. Lett. B **649**, 258 (2007).
17. T. Mersmann et al., Phys. Rev. Lett. **98**, 242301 (2007).
18. C. Wilkin, Phys. Rev. C **47**, R938 (1993).
19. J.C. Peng et al., Phys. Rev. Lett. **63**, 2353 (1989).

Appendix

Table 2. Values in nb/sr of the $pd \rightarrow {}^3\text{He}\pi^0$ differential cross sections shown graphically in Fig. 5 from beam momenta of 1600 MeV/c to 1670 MeV/c. The bins in $z = \cos\vartheta_{\pi^0}^*$ have width 0.016 and the values quoted are the centres of these bins. Statistical uncertainties are given.

z	1600	1610	1620	1630	1640	1650	1660	1670
-0.976	20.4 ± 1.0	19.5 ± 1.0	17.6 ± 0.9	18.3 ± 0.9	20.3 ± 1.0	20.4 ± 1.0	20.0 ± 1.1	20.1 ± 1.0
-0.960	28.1 ± 1.2	24.7 ± 1.0	22.6 ± 1.0	20.5 ± 0.9	20.5 ± 1.0	20.3 ± 0.9	21.7 ± 1.0	21.2 ± 0.9
-0.944	34.1 ± 1.2	31.3 ± 1.1	24.1 ± 1.0	25.2 ± 1.0	24.8 ± 1.0	22.7 ± 0.9	22.7 ± 1.0	23.2 ± 1.0
-0.928	39.9 ± 1.3	33.3 ± 1.1	29.1 ± 1.1	27.9 ± 1.0	29.8 ± 1.1	27.8 ± 1.0	26.7 ± 1.1	26.6 ± 1.0
-0.912	44.2 ± 1.3	40.3 ± 1.1	34.7 ± 1.1	32.1 ± 1.0	34.9 ± 1.1	29.7 ± 1.0	30.2 ± 1.1	28.3 ± 1.0
-0.896	53.4 ± 1.4	45.9 ± 1.2	40.5 ± 1.2	37.0 ± 1.1	38.1 ± 1.2	35.7 ± 1.1	32.6 ± 1.2	32.5 ± 1.1
-0.880	58.8 ± 1.5	51.2 ± 1.3	42.1 ± 1.2	40.6 ± 1.1	41.3 ± 1.2	39.1 ± 1.1	38.3 ± 1.2	34.2 ± 1.1
-0.864	63.0 ± 1.5	55.5 ± 1.3	47.4 ± 1.3	45.1 ± 1.2	46.2 ± 1.3	43.9 ± 1.2	41.0 ± 1.3	40.4 ± 1.2
-0.848	66.6 ± 1.5	58.1 ± 1.3	50.3 ± 1.3	49.7 ± 1.2	48.9 ± 1.3	49.1 ± 1.3	46.9 ± 1.3	42.6 ± 1.2
-0.832	69.2 ± 1.6	61.6 ± 1.4	55.4 ± 1.3	54.9 ± 1.3	54.1 ± 1.4	50.6 ± 1.3	49.8 ± 1.4	45.3 ± 1.3
-0.816	75.1 ± 1.6	64.9 ± 1.4	59.1 ± 1.4	56.0 ± 1.3	58.3 ± 1.4	55.4 ± 1.3	52.6 ± 1.4	47.9 ± 1.3
-0.800	77.9 ± 1.7	69.8 ± 1.5	61.3 ± 1.4	59.1 ± 1.3	59.7 ± 1.4	57.4 ± 1.4	55.3 ± 1.4	52.6 ± 1.3
-0.784	81.4 ± 1.7	70.4 ± 1.5	64.0 ± 1.5	62.0 ± 1.4	61.9 ± 1.4	60.3 ± 1.4	60.0 ± 1.5	56.8 ± 1.3
-0.768	83.0 ± 1.7	75.9 ± 1.5	64.7 ± 1.4	64.7 ± 1.4	68.1 ± 1.5	64.0 ± 1.4	65.0 ± 1.5	58.6 ± 1.4
-0.752	85.4 ± 1.7	78.2 ± 1.5	68.5 ± 1.5	66.8 ± 1.4	68.3 ± 1.5	66.5 ± 1.5	66.6 ± 1.5	61.4 ± 1.4
-0.736	91.7 ± 1.8	78.6 ± 1.5	72.8 ± 1.5	70.0 ± 1.4	74.1 ± 1.5	70.7 ± 1.5	68.4 ± 1.6	65.4 ± 1.4
-0.720	90.5 ± 1.8	80.3 ± 1.5	73.1 ± 1.5	71.1 ± 1.4	73.2 ± 1.5	70.5 ± 1.5	74.4 ± 1.6	68.5 ± 1.4
-0.704	93.6 ± 1.8	83.6 ± 1.6	76.2 ± 1.5	73.4 ± 1.4	77.6 ± 1.6	72.7 ± 1.5	76.4 ± 1.6	70.7 ± 1.5
-0.688	96.2 ± 1.8	85.6 ± 1.6	75.6 ± 1.5	74.8 ± 1.4	77.9 ± 1.6	78.3 ± 1.5	74.0 ± 1.6	72.0 ± 1.5
-0.672	93.9 ± 1.8	86.5 ± 1.6	76.4 ± 1.5	77.0 ± 1.5	79.6 ± 1.6	78.2 ± 1.5	78.2 ± 1.6	74.4 ± 1.5
-0.656	92.4 ± 1.8	88.3 ± 1.6	78.5 ± 1.5	77.2 ± 1.5	79.0 ± 1.6	79.4 ± 1.5	77.4 ± 1.6	77.0 ± 1.5
-0.640	—	87.5 ± 1.6	78.1 ± 1.5	76.8 ± 1.5	79.7 ± 1.6	80.1 ± 1.5	77.6 ± 1.6	75.2 ± 1.5
-0.624	—	—	75.3 ± 1.5	76.6 ± 1.4	82.5 ± 1.6	79.4 ± 1.5	78.2 ± 1.6	77.9 ± 1.5
-0.608	—	—	77.0 ± 1.5	78.5 ± 1.5	83.3 ± 1.6	82.7 ± 1.6	80.3 ± 1.6	76.3 ± 1.5
-0.592	—	—	—	72.4 ± 1.4	82.7 ± 1.6	81.8 ± 1.5	77.4 ± 1.6	76.0 ± 1.5
-0.576	—	—	—	—	79.5 ± 1.6	78.9 ± 1.5	78.2 ± 1.6	77.8 ± 1.5
-0.560	—	—	—	—	—	76.4 ± 1.5	77.6 ± 1.5	74.2 ± 1.4
-0.544	—	—	—	—	—	—	73.2 ± 1.5	74.7 ± 1.4
-0.528	—	—	—	—	—	—	—	70.2 ± 1.4
-0.512	—	—	—	—	—	—	—	67.6 ± 1.4

Table 3. Values in nb/sr of the $pd \rightarrow {}^3\text{He}\pi^0$ differential cross sections shown graphically in Fig. 5 from beam momenta of 1680 MeV/c to 1740 MeV/c. The bins in $z = \cos\vartheta_{\pi^0}^*$ have width 0.016 and the values quoted are the centres of these bins. Statistical uncertainties are given.

z	1680	1690	1700	1710	1720	1730	1740
-0.976	19.0 ± 1.0	21.0 ± 1.0	21.6 ± 0.6	22.8 ± 1.0	21.4 ± 1.2	24.1 ± 1.1	22.6 ± 1.1
-0.960	19.9 ± 1.0	20.2 ± 0.9	19.8 ± 0.5	19.9 ± 1.0	19.7 ± 1.1	20.3 ± 0.9	20.2 ± 1.0
-0.944	20.2 ± 1.0	21.7 ± 0.9	19.5 ± 0.5	20.0 ± 1.0	21.3 ± 1.0	19.9 ± 0.9	17.2 ± 0.9
-0.928	23.4 ± 1.0	23.2 ± 0.9	20.1 ± 0.5	20.0 ± 0.9	21.1 ± 1.0	19.3 ± 0.9	18.8 ± 0.9
-0.912	24.8 ± 1.0	23.5 ± 0.9	21.9 ± 0.5	21.0 ± 0.9	22.3 ± 1.0	19.9 ± 0.9	19.0 ± 1.0
-0.896	28.9 ± 1.1	27.7 ± 1.0	23.6 ± 0.6	23.9 ± 1.0	23.7 ± 1.0	21.5 ± 0.9	21.5 ± 1.0
-0.880	31.2 ± 1.1	28.2 ± 1.0	25.5 ± 0.6	24.8 ± 1.0	25.3 ± 1.1	21.7 ± 0.9	22.1 ± 1.0
-0.864	38.1 ± 1.2	31.9 ± 1.1	28.5 ± 0.6	30.1 ± 1.1	29.0 ± 1.1	24.0 ± 1.0	25.6 ± 1.0
-0.848	38.4 ± 1.2	33.6 ± 1.1	32.4 ± 0.6	31.1 ± 1.1	30.3 ± 1.1	27.3 ± 1.0	27.4 ± 1.1
-0.832	42.4 ± 1.3	39.9 ± 1.2	36.1 ± 0.7	36.3 ± 1.2	34.5 ± 1.2	29.3 ± 1.1	29.1 ± 1.1
-0.816	46.9 ± 1.3	44.1 ± 1.2	37.9 ± 0.7	39.2 ± 1.2	38.2 ± 1.3	32.2 ± 1.1	31.3 ± 1.1
-0.800	48.2 ± 1.3	47.9 ± 1.2	40.8 ± 0.7	43.8 ± 1.3	40.9 ± 1.3	34.6 ± 1.1	36.4 ± 1.2
-0.784	53.4 ± 1.4	50.3 ± 1.3	43.2 ± 0.7	46.1 ± 1.3	44.9 ± 1.3	39.0 ± 1.2	37.6 ± 1.2
-0.768	57.7 ± 1.4	54.3 ± 1.3	46.6 ± 0.7	46.8 ± 1.3	47.5 ± 1.4	42.9 ± 1.2	40.5 ± 1.2
-0.752	62.3 ± 1.5	55.3 ± 1.3	50.2 ± 0.8	50.0 ± 1.3	51.0 ± 1.4	45.7 ± 1.2	46.3 ± 1.3
-0.736	63.4 ± 1.5	59.4 ± 1.4	53.8 ± 0.8	54.0 ± 1.4	55.7 ± 1.5	48.5 ± 1.3	48.6 ± 1.3
-0.720	68.8 ± 1.5	62.3 ± 1.4	56.5 ± 0.8	57.9 ± 1.4	55.9 ± 1.4	51.3 ± 1.3	51.6 ± 1.4
-0.704	69.8 ± 1.5	66.6 ± 1.4	58.8 ± 0.8	62.4 ± 1.4	59.6 ± 1.5	53.6 ± 1.3	53.4 ± 1.4
-0.688	69.5 ± 1.5	68.8 ± 1.4	60.0 ± 0.8	61.1 ± 1.4	60.8 ± 1.5	55.4 ± 1.3	57.8 ± 1.4
-0.672	71.1 ± 1.5	68.2 ± 1.4	60.8 ± 0.8	65.8 ± 1.5	63.6 ± 1.5	57.0 ± 1.3	59.8 ± 1.4
-0.656	75.2 ± 1.6	68.7 ± 1.4	62.0 ± 0.8	65.2 ± 1.5	62.9 ± 1.5	58.4 ± 1.3	58.6 ± 1.4
-0.640	75.7 ± 1.6	69.8 ± 1.4	60.9 ± 0.8	68.7 ± 1.5	65.6 ± 1.5	58.9 ± 1.3	59.7 ± 1.4
-0.624	76.5 ± 1.6	68.9 ± 1.4	63.2 ± 0.8	66.2 ± 1.4	65.2 ± 1.5	60.4 ± 1.4	60.5 ± 1.4
-0.608	77.7 ± 1.6	68.8 ± 1.4	62.5 ± 0.8	64.9 ± 1.4	65.4 ± 1.5	59.9 ± 1.3	60.5 ± 1.4
-0.592	74.9 ± 1.5	67.7 ± 1.4	62.2 ± 0.8	66.7 ± 1.4	63.4 ± 1.5	59.5 ± 1.3	60.5 ± 1.4
-0.576	79.1 ± 1.6	68.1 ± 1.4	61.5 ± 0.8	68.3 ± 1.4	63.9 ± 1.5	60.7 ± 1.3	58.6 ± 1.4
-0.560	75.6 ± 1.6	65.9 ± 1.3	59.1 ± 0.8	63.6 ± 1.4	63.5 ± 1.4	57.8 ± 1.3	56.8 ± 1.4
-0.544	77.2 ± 1.6	64.6 ± 1.3	59.4 ± 0.8	63.4 ± 1.4	61.3 ± 1.4	58.4 ± 1.3	56.0 ± 1.3
-0.528	73.7 ± 1.5	63.5 ± 1.3	56.4 ± 0.7	60.0 ± 1.3	58.0 ± 1.3	58.8 ± 1.3	52.0 ± 1.3
-0.512	70.1 ± 1.5	60.4 ± 1.2	54.9 ± 0.7	60.4 ± 1.3	55.8 ± 1.3	56.3 ± 1.3	50.9 ± 1.2
-0.496	66.4 ± 1.4	61.5 ± 1.2	51.1 ± 0.7	55.6 ± 1.3	55.6 ± 1.3	51.7 ± 1.2	48.5 ± 1.2
-0.480	—	53.0 ± 1.2	49.7 ± 0.7	52.4 ± 1.2	50.7 ± 1.2	47.7 ± 1.1	43.1 ± 1.1
-0.464	—	—	44.2 ± 0.6	46.2 ± 1.1	47.3 ± 1.2	43.9 ± 1.1	40.2 ± 1.1
-0.448	—	—	—	40.8 ± 1.0	41.4 ± 1.1	40.3 ± 1.1	37.2 ± 1.0
-0.432	—	—	—	—	35.8 ± 1.0	36.0 ± 1.0	30.6 ± 0.9
-0.416	—	—	—	—	—	27.4 ± 0.9	25.9 ± 0.8